Three-Dimensional Fluorescence Recovery after Photobleaching with the Confocal Scanning Laser Microscope

Kevin Braeckmans, Liesbeth Peeters, Niek N. Sanders, Stefaan C. De Smedt, and Joseph Demeester
Laboratory of General Biochemistry and Physical Pharmacy, Ghent University, Ghent, Belgium

ABSTRACT Confocal scanning laser microscopes (CSLMs) are equipped with the feature to photobleach user-defined regions. This makes them a handy tool to perform fluorescence recovery after photobleaching (FRAP) measurements. To allow quantification of such FRAP experiments, a three-dimensional model has been developed that describes the fluorescence recovery process for a disk-shaped geometry that is photobleached by the scanning beam of a CSLM. First the general mathematical basis is outlined describing the bleaching process for an arbitrary geometry bleached by a scanning laser beam. Next, these general expressions are applied to the bleaching by a CSLM of a disk-shaped geometry and an analytical solution is derived that describes three-dimensional fluorescence recovery in the bleached area as observed by the CSLM. The FRAP model is validated through both the Stokes-Einstein relation and the comparison of the measured diffusion coefficients with their theoretical estimates. Finally, the FRAP model is used to characterize the transport of FITC-dextrans through bulk three-dimensional biological materials: vitreous body isolated from bovine eyes, and lung sputum expectorated by cystic fibrosis patients. The decrease in the diffusion coefficient relative to its value in solution was dependent on the size of the FITC-dextrans in vitreous, whereas it was size-independent in cystic fibrosis sputum.

INTRODUCTION

Recent advancements in the biomedical and pharmaceutical field have stimulated the development of macromolecular therapeutics (Crystal, 1995; Cho and Juliano, 1996; Rojanasakul, 1996) and colloidal nanoscopic drug carriers (Weers, 1998; Torchilin, 2000). The delivery and the transport of macromolecular therapeutics and colloidal drug carriers in vivo requires overcoming major biological barriers (Sanders et al., 2000). For example, nanoscopic liposome/DNA complexes for gene therapy of cystic fibrosis (CF) have to cross the mucus layer in the patient's lungs before being effective (Sanders et al., 2001, 2002a,b). Also, anticancer drugs entrapped in nanoscopic carriers have to move within the tumor interstitial matrix, which acts as a barrier to drug delivery (Brown et al., 2000; Pluen et al., 2001; Ramanujan et al., 2002; Campbell et al., 2002).

An ideal tool for studying the mobility characteristics of molecules and particles on a microscopic level is fluorescence recovery after photobleaching (FRAP). For a long time FRAP has been successfully used to assess the translational mobility of all kinds of solutes in cytoplasm, nuclei, and membranes (Edidin, 1992; Ishihara and Jacobson, 1993; Seksek et al., 1997; Umenishi et al., 2000). Besides its cellular applications, FRAP has also been used to study the mobility of molecules in interstitial spaces of (tumor) tissues (Chary and Jain, 1989; Ramanujan et al., 2002) and extracellular matrices such as cervical mucus and biofilms (Saltzman et al., 1994; Sanders et al., 2000; Olmsted et al., 2001). For an extensive review covering many applications of FRAP and its advantages over other techniques for the measurement of diffusion coefficients, see Meyvis et al. (1999).

FRAP models for use with regular (i.e., nonscanning) fluorescence microscopes have already been developed. They describe the relation between the diffusion into a two-dimensional (2-D) bleached region and the fluorescence recovery as observed by the fluorescence microscope (Axelrod et al., 1976; Soumpasis, 1983; Lopez et al., 1988; Tsay and Jacobson, 1991; Berk et al., 1993; Gordon et al., 1995). Nowadays, however, bleaching experiments can be easily carried out on confocal scanning laser microscopes (CSLMs) as they are often equipped with the feature to bleach arbitrary regions in the sample. When the bleaching geometry is defined in the software, the microscope scans the laser beam over the sample in a raster pattern, pixel-by-pixel and line-by-line, while modulating the beam intensity according to the designed pattern. The ability to bleach arbitrary regions makes such CSLMs an excellent standard tool to perform FRAP experiments.

Few FRAP models exist, however, for use with a CSLM. A model based on a statistical evaluation of the fluorescence inside the bleached region has been reported, but the analysis was limited to 2-D samples (Kubitscheck et al., 1994). Both two-dimensional and three-dimensional models have been developed as well, based on a numerical approach (Wedekind et al., 1994, 1996; Kubitscheck et al., 1998; Peters and Kubitscheck, 1999), but due to the complicated and often time-consuming computations involved, the practical use of this model seems limited. An approximate but very practical three-dimensional (3-D) model has been developed for use with objective lenses of low numerical aperture (NA) on a CSLM (Blonk et al., 1993). This method relies on a specially adapted CSLM and uses a *stationary* laser beam for bleaching and a line-scanning beam for recording the fluorescence recovery. This sequence of

Submitted April 30, 2003, and accepted for publication July 16, 2003.

Address reprint requests to Stefaan C. De Smedt, E-mail: stefaan.desmedt@ugent.be.

0006-3495/03/10/2240/13 $2.00

scanning modes appears not always to be possible on commercial CSLMs, which are rather equipped with the possibility to bleach 2-D geometries by a *scanning* beam. Therefore, it would be an advantage to have a FRAP model that can readily be applied on such standard CSLMs. Additionally, to allow general and widespread use of the model, it should be based on ''simple'' mathematics that can be easily programmed in a standard fitting routine and with instant computation times.

Here we present such a new FRAP model that can be easily applied on almost any modern CSLM equipped with the feature to bleach arbitrary regions. An outline of the general mathematical basis will be given first which describes the bleaching process for a geometry bleached by a scanning laser beam. Next, the analytical solution will be derived that describes 3-D fluorescence recovery as observed by the confocal microscope after bleaching of disk-shaped geometry. After extensive experimental evaluation, the new FRAP model will be used to characterize the diffusion of fluorescent dextrans in vitreous body isolated from bovine eyes and lung sputum expectorated by cystic fibrosis (CF) patients.

THEORETICAL FRAMEWORK: DERIVATION OF THE FRAP MODEL

Bleaching a geometry with a scanning beam

When a geometry is bleached by a CSLM, it is done sequentially, pixel-by-pixel and line-by-line. We will assume that the bleaching phase is very short so that the amount of fluorescence recovery that will take place during bleaching is negligible. Furthermore, it is assumed that the bleaching reaction can be described by an irreversible first-order reaction,

$$\frac{\partial C(x,y,z,t)}{\partial t} = -\alpha I_b(x,y,z)C(x,y,z,t), \qquad (1)$$

where $C(x,y,z,t)$ is the spatial concentration of fluorophores at a time t, α is the bleach rate which is specific for a certain type of fluorophore in a particular medium, and $I_b(x,y,z)$ is the 3-D intensity distribution of the bleaching beam. In a CSLM, the light source is a laser beam focused down through an objective lens and the resulting 3-D intensity distribution is called the point-spread function (PSF) (Cogswell and Larkin, 1995; Keller, 1995). From now on we will therefore simply refer to $I_b(x,y,z)$ as the *bleaching PSF*. To describe the bleaching phase in the case of a CSLM, Eq. 1 has to be solved for the bleaching PSF being scanned across the sample according to a certain 2-D geometry. Since a 2-D geometry is scanned sequentially line-by-line, it is instructive to first consider the case of the bleaching of a single line segment (see Appendix A). These results can subsequently be extended to the general 2-D case as explained in Appendix B, where it is found that the concentration of fluorophores after bleaching of a 2-D geometry $B(x,y)$ by scanning of the bleaching PSF $I_b(x,y,z)$ can be calculated from

$$C_b(x,y,z) = C_0(x,y,z)e^{-(\alpha/v\Delta y)K(x,y,z)}, \qquad (2)$$

where v is the constant line scanning speed and Δy is the distance between two adjacent scanning lines (see Fig. 1), and where it is understood that Δy is smaller than one-half the resolution of the bleaching PSF. $K(x,y,z)$ is the bleaching light distribution which results from scanning the bleaching geometry with the bleaching PSF and can be calculated from the convolution product of $B(x,y)$ and $I_b(x,y,z)$:

$$K(x,y,z) = B(x,y) \otimes I_b(x,y,z) = \int_{-\infty}^{+\infty}\int_{-\infty}^{+\infty} B(x',y')I_b(x-x',y-y',z)dx'dy'. \qquad (3)$$

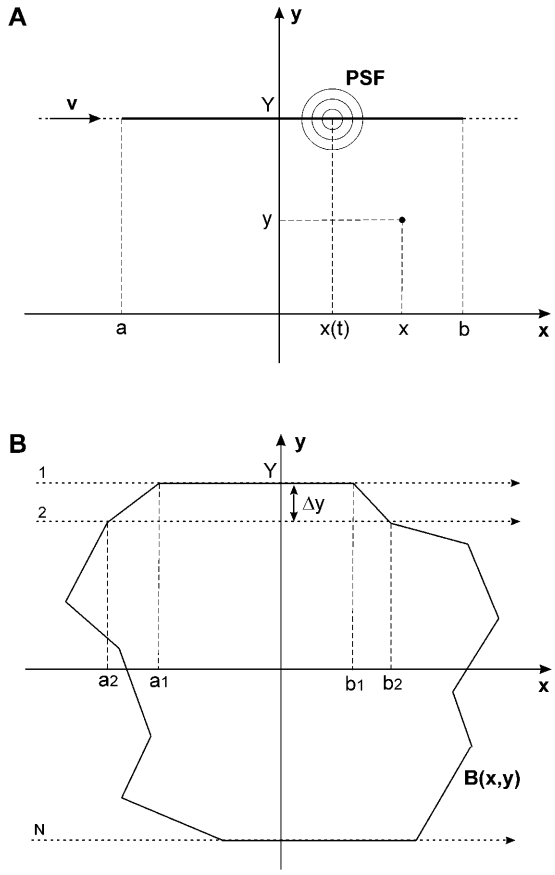

FIGURE 1 (*A*) The bleaching PSF $I_b(x,y,z)$ is scanned with constant scanning speed v across a line $y = Y$. The light intensity is zero, except from position $x = a$ to $x = b$. (*B*) A 2-D geometry $B(x,y)$ is bleached by scanning N adjacent line segments. The laser intensity is at a certain level within the geometry's boundaries and zero outside. The origin is chosen arbitrarily, whereas the x-axis is parallel to the line scanning direction. The first line $y = Y$ is bleached from position $x = a_i$ to $x = b_i$, whereas the i^{th} line $y = Y - (i-1)\Delta y$ is bleached from $x = a_i$ to $x = b_i$.

From Eq. 2 it can be seen that the scanning speed v and the distance between the adjacent bleach lines Δy play an important role in the amount of bleaching. It is worth noting that on a CSLM instrument, both parameters can be varied by changing the electronic *zoom factor*. Zoom 1 corresponds to the full field of view, whereas, for example at zoom 2, only one-half the full distance in the x- and y-directions is scanned. This means that at zoom 2 the line-scanning speed v and the interline distance Δy will be only one-half their value at zoom 1. Therefore, if v_0 and Δy_0 are respectively the scanning speed and interline distance at zoom 1, then at zoom Z the scanning speed, $v = v_0/Z$, and the interline distance, $\Delta y = \Delta y_0/Z$, and Eq. 2 can be rewritten as

$$C_b(x,y,z) = C_0(x,y,z)e^{-(\alpha Z^2/v_0\Delta y_0)K(x,y,z)}, \quad (4)$$

explicitly showing the strong dependence of the amount of bleaching on the zoom setting.

Bleaching of a disk by a scanning beam

Now we will apply Eq. 2 for the bleaching of an arbitrary geometry to the special case of a disk with radius w and a constant bleaching intensity. In this case, the geometry $B(r)$ in cylindrical coordinates is

$$B(r) = \begin{cases} 1 & \text{if } r \le w \\ 0 & \text{if } r > w \end{cases}. \quad (5)$$

Analogous to previous theoretical work on FRAP in three dimensions (Blonk et al., 1993), we take the bleaching PSF, $I_b(x,y,z)$, to be radially and axially Gaussian distributed, with respective resolutions r_0 and z_0:

$$I_b(x,y,z) = I_{0b}e^{-2(x^2+y^2/r_0^2)}e^{-2(z^2/z_0^2)}. \quad (6)$$

It should be noted that the radial resolution r_0 is considered to be independent of the axial coordinate z. As a consequence, Eq. 6 is valid only for lenses of relatively low NA (which have a cylindrical illumination profile). Lenses of high NA have a conical shape and the radial resolution will be a function of the axial coordinate z (Kubitscheck et al., 1998). However, a more complicated PSF such as this will prevent us from finding an analytical solution for the recovery process, which is one of the objectives of this study. Therefore, we will continue with Eq. 6, realizing this derivation in 3-D is only valid for lenses of low NA. If the disk's radius w is much larger than the radial resolution r_0, the PSF may be considered to have a negligible radial resolution and can be approximated by

$$I_b(x,y,z) = I_{0b}\delta(x,y)e^{-2(z^2/z_0^2)}, \quad (7)$$

where $\delta(x,y)$ is the Dirac delta function. How small the radial resolution will have to be compared to the bleaching disk's radius for this assumption to be true, will have to be determined experimentally (see Results and Discussion). By substitution of Eqs. 5 and 7 into Eq. 3, it follows that the resulting bleaching light distribution $K(r,z)$ in cylindrical coordinates is

$$K(r,z) = \begin{cases} I_{0b}e^{-2(z^2/z_0^2)} & \text{if } r \le w \\ 0 & \text{if } r > w \end{cases}, \quad (8)$$

which is a cylindrical illumination profile of radius w with a uniform radial and a Gaussian axial distribution. Eq. 8 leads to the important conclusion that, if a disk is scanned whose radius w is much larger than the radial resolution of the bleaching PSF, the resulting bleaching illumination profile is equivalent to that of a stationary beam with a uniform radial and a Gaussian axial distribution, with respective resolutions w and z_0. Therefore, we will refer to the new FRAP model as the *uniform disk model*. The 3-D fluorophore concentration distribution after bleaching of a uniform disk by a scanning beam is finally found from Eqs. 2 and 8,

$$C_b(r,z) = \begin{cases} C_0(r,z)e^{-K_0 e^{-2(z^2/z_0^2)}} & \text{if } r \le w \\ C_0(r,z) & \text{if } r > w \end{cases}, \quad (9)$$

where we have defined the bleaching parameter

$$K_0 = \frac{\alpha I_{0b}}{v\Delta y},$$

which determines the bleaching depth. From Eq. 4 it immediately follows that the bleaching parameter can be explicitly written in terms of the zoom setting Z of the CSLM as well:

$$K_0 = \frac{\alpha I_{0b}Z^2}{v_0\Delta y_0}.$$

To have a good understanding of the assumption made in Eq. 7 and its implications, let us examine the difference between the discontinuous approximation Eq. 8 and the exact solution for $K(x,y,z)$, which can be calculated from Eqs. 5 and 6 (formula not shown). Both the exact and approximate intensity distributions are plotted in Fig. 2 *A* for three disks of radii, $w = r_0$, $w = 3r_0$, and $w = 5r_0$. It is clear that, the larger the radius w compared to the bleaching resolution r_0, the better the approximation Eq. 8 will be valid. It is also important to note that, if the concentration after bleaching is calculated with the exact solution for $K(x,y,z)$, the radius of the disk (at full-width half-maximum, i.e., FWHM) tends to increase slightly with increasing bleaching parameter K_0 because of the slope at the edges and the exponential process. Examples for a disk of radius $w = 5r_0$ are shown in Fig. 2 *B* for three different K_0 values, together with their best discontinuous approximation at the FWHM position. Based on such simulations we have determined an approximate relation between the bleaching parameter K_0 and the increase in length Δw of the bleaching disk's radius relative to the resolution r_0 of the bleaching PSF. These results are shown

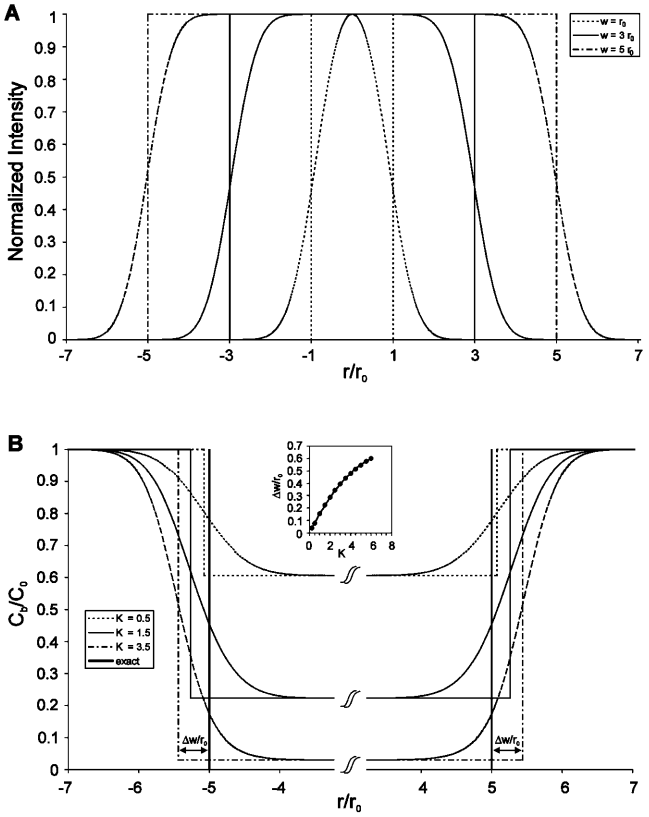

FIGURE 2 (*A*) When scanning a disk of radius w, the edges of the resulting light distribution show a slope that extend over a certain distance in space because of the radial Gaussian distribution of the bleaching PSF. The larger the radius w compared to the radial resolution r_0 of the bleaching PSF, the better the radial intensity profile can be approximated by a discontinuous step function which is 1 inside the bleaching disk and zero outside. The exact radial illumination profile together with the discontinuous approximation are plotted for three different radii: $w = r_0$, $w = 3r_0$, and $w = 5r_0$. It is clear that, the larger the radius w, the better the discontinuous approximation will be valid. (*B*) The exact bleaching profile for a disk of radius $w = 5r_0$ has been calculated for different values of the bleaching parameter: $K_0 = 0.5$, 1.5, and 3.5. The bold lines at $r = -5r_0$ and $r = 5r_0$ indicate the bleaching disk's boundaries. For each of the bleaching profiles the best discontinuous approximation is drawn as well with edges at the FWHM. As can be seen, based on the positions of the FWHM, the effective radius of the bleached disk becomes larger with increasing bleaching depth. The increase in length $\Delta w/r_0$ is indicated at each side of the profile for $K_0 = 3.5$. In the inset, the increase in length $\Delta w/r_0$ of the bleaching disk's radius w is plotted as a function of the bleaching parameter K_0. A second-degree polynomial seems to describe well this relationship for $0 \le K_0 \le 6$.

in the inset of Fig. 2 *B*, leading to the following relation (based on a best fit of a second-degree polynomial):

$$\frac{\Delta w}{r_0} = -0.0106K_0^2 + 0.163K_0 \quad (0 \le K_0 \le 6). \tag{10}$$

If one wants to obtain the diffusion coefficient with the highest possible accuracy, it will be necessary to take Eq. 10 into account. In the Results and Discussion section we will demonstrate the effect of taking Eq. 10 into account or not.

Three-dimensional fluorescence recovery after bleaching of a uniform disk

After (the instantaneous) photobleaching of a uniform disk, the bleached molecules will start to diffuse out of the bleached volume and will be replaced by diffusion of unbleached fluorophores into the bleached volume. The fluorophore concentration distribution at a time t after bleaching can be calculated by solving Fick's second law in cylindrical coordinates (Crank, 1975),

$$\frac{1}{D}\frac{\partial}{\partial t}C(r,z,t) = \left(\frac{\partial^2}{\partial r^2} + \frac{1}{r}\frac{\partial}{\partial r}\right)C(r,z,t) + \frac{\partial^2}{\partial z^2}C(r,z,t), \tag{11}$$

for the initial condition Eq. 9. Next, the total fluorescence, $F_{\mathrm{tot}}(t)$, inside the disk can be calculated as observed by the CSLM when using a strongly attenuated detection beam. The 3-D intensity distribution $I_{\mathrm{d}}(x,y,z)$ of the detection beam focused through the objective lens will be termed the *detection PSF*. $I_{\mathrm{d}}(x,y,z)$ is considered to be of the same form as the bleaching PSF $I_{\mathrm{b}}(x,y,z)$, except for the intensity which is $A\times$ smaller than the bleaching intensity:

$$I_{\mathrm{d}}(x,y,z) = \frac{1}{A}I_{\mathrm{b}}(x,y,z).$$

Again, assuming that the resolution of the detecting PSF is much smaller than the radius of the bleaching disk, it is finally found (see Appendix C) that the total fluorescence inside the bleached disk can be calculated from

$$\frac{F_{\mathrm{tot}}(t)}{F_0} = 1 + \frac{1}{\mathrm{erf}\left(\sqrt{2}\frac{\Delta z_0}{z_0}\right)} \times \left\{\sum_{n=1}^{+\infty}\left[\frac{(-K_0)^n}{n!}\frac{1}{\sqrt{\alpha_n}}\mathrm{erf}\left(\sqrt{\frac{2\alpha_n}{\alpha_n - n}}\frac{\Delta z_0}{z_0}\right)\right] \times \left(1 - e^{-2(\tau_{\mathrm{r}}/t)}\left(\mathrm{I}_0\left(2\frac{\tau_{\mathrm{r}}}{t}\right) + \mathrm{I}_1\left(2\frac{\tau_{\mathrm{r}}}{t}\right)\right)\right)\right\}, \tag{12}$$

where F_0 is the total fluorescence inside the disk before bleaching; Δz_0 a parameter taking a finite confocal pinhole aperture into account by rejecting fluorescence light from planes above Δz_0 and below $-\Delta z_0$; I_0 and I_1 are the modified Bessel functions of 0^{th} and first order; K_0 is the bleaching parameter $\alpha_{\mathrm{n}} = 1+n(1+(2t/\tau_{\mathrm{z}}))$; $\tau_{\mathrm{r}} = (w^2/4D)$ the radial characteristic diffusion time; and $\tau_{\mathrm{z}} = (z_0^2/4D)$ is the axial characteristic diffusion time. In the case of a fully opened confocal aperture ($\Delta z_0 \to +\infty$), the error functions reach unity and Eq. 12 becomes

$$\frac{F_{\mathrm{tot}}(t)}{F_0} = 1 + \left\{\sum_{n=1}^{+\infty}\left[\frac{(-K_0)^{\mathrm{n}}}{n!}\frac{1}{\sqrt{\alpha_{\mathrm{n}}}}\right] \times \left(1 - e^{-2(\tau_{\mathrm{r}}/t)}\left(\mathrm{I}_0\left(2\frac{\tau_{\mathrm{r}}}{t}\right) + \mathrm{I}_1\left(2\frac{\tau_{\mathrm{r}}}{t}\right)\right)\right)\right\}, \tag{13}$$

and for $z_0 \rightarrow +\infty$ (low NA), Eq. 13 reduces to

$$\frac{F_{\text{tot}}(t)}{F_0} = 1 + \left\{ \sum_{n=1}^{+\infty} \left[\frac{(-K_0)^n}{n!} \frac{1}{\sqrt{1+n}} \right] \times \left(1 - e^{-2(\tau_r/t)} \left(\text{I}_0\left(2\frac{\tau_r}{t}\right) + \text{I}_1\left(2\frac{\tau_r}{t}\right) \right) \right) \right\}. \quad (14)$$

In fact, it can be shown that Eq. 14 is true for any value of Δz_0 (and not just for $\Delta z_0 \rightarrow +\infty$), and hence it is independent of the confocal aperture. It is important to note that Eq. 14 is equivalent to the expression of Soumpasis (1983) for 2-D diffusion in the case of a *stationary* bleaching beam with uniform radial intensity distribution, except that we have explicitly taken the bleaching depth into account. This leads to the important conclusion that, for objective lenses of low numerical aperture (for which $z_0 \rightarrow +\infty$), the 3-D Eq. 12 for a disk bleached by a *scanning* beam reduces to the simpler 2-D formula for a uniform disk bleached by a *stationary* beam (Soumpasis, 1983). It also follows that Eq. 12 can be considered to be a 3-D expansion of the already known 2-D formula for a uniform disk bleached by a *stationary* beam.

In this work we will use relatively low NA lenses (NA $\approx$ 0.2) for which we have seen that the 3-D Eq. 12 does not give more accurate results than Eq. 14 for the 2-D case. For lenses of slightly higher NA (NA $\approx$ 0.5) it is expected that Eq. 12 will be needed instead. We also recall at this point that the 3-D expression Eq. 12 will not be valid for lenses of high NA. However, the 2-D expression Eq. 14 will be valid for lenses of high NA as well if the sample is thin compared to the axial resolution of the scanning beam. In that case there will be uniform bleaching along the z-axis throughout the sample and the diffusion is restricted to two dimensions.

Eqs. 12–14 are valid if all molecules are mobile. In practice, however, there can be a mobile fraction k (and an immobile fraction $1-k$). To take such a mobile fraction k into account, these expressions have to be substituted into the right part of

$$\frac{F_{\text{tot}}(z,t)}{F_{\text{tot}}(z,0)} = 1 + k\left(\frac{F_{\text{tot}}(z,t)}{F_{\text{tot}}(z,0)} - 1 \right). \quad (15)$$

Let it be noted that for numerical computations, Eq. 14 cannot be used to calculate the fluorescence at $t = 0$ (i.e., immediately after bleaching). Instead, the expression

$$\frac{F_{\text{tot}}(0)}{F_0} = 1 + \sum_{n=1}^{+\infty} \left[\frac{(-K_0)^n}{n!} \frac{1}{\sqrt{1+n}} \right]$$

should be used, which is readily found from Eq. 14, by making use of the large argument asymptotic expansion of

$$e^{-2(\tau_r/t)} \left(\text{I}_0\left(2\frac{\tau_r}{t}\right) + \text{I}_1\left(2\frac{\tau_r}{t}\right) \right).$$

In the derivation of the FRAP model we have made a number of assumptions that are to be met by the experimental conditions:

1. The fluorescent molecules in the sample have to be initially uniformly distributed. This means that there should be no concentration gradient present before bleaching.
2. The diffusion process has been assumed to be isotropic and to take place in an infinite medium. In practice, the latter condition means that during the time period over which the recovery is observed, the diffusion front should not have reached any boundaries at which it will be reflected and influence the free diffusion process (Crank, 1975). By examining the sample with the confocal microscope, the user can choose an area that fulfills these requirements.
3. An objective lens of low NA should be used for bleaching and observation of the fluorescence recovery in a 3-D sample. Lenses of high NA can be used in combination with the 2-D expressions if the thickness of the sample is small compared to the axial resolution of the lens, in which case the diffusion is restricted to two dimensions.
4. The bleaching phase has to be sufficiently short to avoid recovery during bleaching. As a rule of thumb, the total bleaching time should be at least 15× smaller than the characteristic recovery time (Meyvis et al., 1999).
5. Finally, there should be no flow present in the medium that can contribute to the fluorescence recovery, which can be checked by examining the position of the bleached disk in the recovery images.

MATERIALS AND METHODS

FRAP equipment

The FRAP experiments are performed on a CSLM (model MRC1024 UV, Bio-Rad, Hemel Hempstead, UK) modified to be able to bleach arbitrary regions (Wedekind et al., 1994; Braeckmans et al., 2003). All bleaching experiments have been performed with the 488-nm line of a 4 W Ar-ion laser (model Stabilite 2017; Spectra-Physics, Darmstadt, Germany). In general, the intensity of the bleaching beam is 1000–10,000× higher than the detection beam. Typical bleaching powers in the sample range from 1 to 15 mW. A 10× objective lens (CFI Plan Apochromat; Nikon, Badhoevedorp, The Netherlands) with a numerical aperture (NA) of 0.45 was used. On the Bio-Rad MRC1024, however, the back aperture of this lens is only partially filled, resulting in a lower effective NA of ~0.2 and an increased resolution of $r_0 = 1.4$ μm (instead of ~700 nm as expected theoretically).

Test solutions

Before performing FRAP measurements on solutions of a fluorophore, the concentration range has to be determined in which a linear relation exists between the observed fluorescence and the concentration of the fluorophore. Based on the outcome of such experiments on FITC-dextran (Sigma-Aldrich, Bornem, Belgium) solutions (prepared in HEPES buffer at pH 7.4),

the following concentrations have been chosen: 2 mg/ml for FITC-dextran $M_w = 2 \times 10^6$ g/mol, which will be referred to as FD2000; 1.5 mg/ml for FITC-dextran $M_w = 4.64 \times 10^5$ g/mol, which will be referred to as FD464; 4 mg/ml for FITC-dextran $M_w = 1.67 \times 10^5$ g/mol, which will be referred to as FD167. Next, FITC-dextran solutions were prepared in HEPES buffer containing varying amounts of glucose. The glucose was used to vary the dynamic viscosity of the FITC-dextran solutions. The dynamic viscosity η [Ns/m^2] for each of the solutions was determined by measuring its density ρ [kg/m^3] and kinematic viscosity ν [m^2/s] and making use of the relation $\eta = \rho \times \nu$. The kinematic viscosity was measured with a capillary viscosimeter (model PVS1; Lauda Dr. R. Wobser GmbH & CO. KG, Lauda-Königshofen, Germany). The density was determined with a picnometer.

FRAP experiments were performed on the FITC-dextran solutions in borosilicate microcapillaries (Vitrocom, Mountain Lakes, NJ) with square cross-section (300 μm $\times$ 300 μm inner dimensions, 5-cm long, wall thickness of 150 μm) to eliminate any currents in the solution while retaining a 3-D environment for the diffusion to take place.

Bovine vitreous

Vitreous gel was dissected from bovine eyes obtained from the local abattoir. For each FRAP experiment, ~200 μl of vitreous from an individual eye was put in a cuvette with a glass bottom for use with an inverted microscope (Nalge Nunc International, Naperville, IL). 30 μl of the FITC-dextran solutions (described above) was injected at several locations near the center of the vitreous gel with a needle. The samples were stirred by hand with a plastic rod at least 10×. The fluorescent solution was allowed to spread throughout the sample for 30–60 min before performing FRAP experiments. FRAP measurements were performed in those regions of the sample that showed the lowest fluorescence signal to make sure that measurements were performed in the vitreous gel and not in or near one of the injection sites.

Cystic fibrosis sputum

Approval for the collection of cystic fibrosis (CF) sputum was obtained from the Ethics Committee of the University Hospital of Ghent. The sputum was expectorated by CF patients during chest physiotherapy. Details on the collection and storage of the CF sputum have been described previously (Sanders et al., 2000).

Fluorescent (yellow-green) polystyrene nanospheres of different sizes, bearing carboxyl groups on their surface, were obtained from Molecular Probes (Leiden, The Netherlands). The weight-average hydrodynamic diameters, measured by dynamic light scattering, of the nanospheres diluted in distilled water were 37 nm $\pm$ 2 nm, and 89 nm $\pm$ 2 nm. The fluorescent nanospheres, diluted in ''sputum buffer'' (85 mM Na^+, 75 mM Cl^-, 3 mM Ca^{2+}, and 20 mM HEPES pH 7.4), and the FITC-dextran solutions were gently mixed with the freshly collected CF sputa and incubated overnight at 4°C. The final concentration of the nanospheres in the CF sputum was 4.02 $\times 10^{12}$ particles/ml for the 37 nm particles and 4.45 $\times 10^{12}$ particles/ml for the 89 nm particles. The final concentration of the FITC-dextrans in the CF sputum was 0.36, 0.14, and 0.18 mg/ml for FD167, FD464, and FD2000, respectively.

To perform FRAP experiments, the CF sputum containing the FITC-dextrans or nanospheres was sandwiched between a microscope slide and a coverslip sealed by two adhesive spacers of 120-μm thickness each (Secure-Seal Spacer; Molecular Probes, Leiden, The Netherlands) in between.

Experimental FRAP protocol

The sample is at first positioned on the microscope stage and the location of interest is brought into focus. As Eq. 14 is independent of the confocal diaphragm setting, it is opened completely to detect as much fluorescence light as possible with a low power illumination beam and to minimize bleaching when recording the fluorescence recovery. After a disk of a particular diameter has been drawn in the bleaching software, a time-series is recorded with the CSLM resulting in a stack of images (see Fig. 3 *A*). The first image of the series shows the sample before bleaching, the second one shows the disk at the time of bleaching, and the subsequent images show the recovery process after bleaching. The time interval between the images is user-defined, with a minimum of 2.13 s for our confocal microscope at 512 $\times$ 512 pixels per image and normal scanning speed. The choice of this time period will depend on the recovery speed. Usually, we have recorded stacks of 30 images with a time interval between 2.5 s and 60 s.

Data extraction and fitting

An image processing program was written to extract the experimental recovery curve from the stack of images. The data extraction is based on the following calculations. First, the position of the bleached disk is analyzed by a center-of-mass algorithm that determines the center of the bleached disk for each of the images. This allows checking for any displacement by flow in the sample. Second, each of the recovery images is normalized to the first image, the prebleach image. To prevent an increase in noise due to this process, each of the images is first smoothed by a 3 $\times$ 3 convolution mask. Next, the mean fluorescence intensity inside the disk is calculated for each image. To correct for any bleaching that might have occurred during the recording of the recovery phase, this value is normalized to the mean fluorescence intensity of one or more user-defined background regions. Finally, the experimental parameters are determined by a least-squares fit of Eqs. 10, 14, and 15 to the experimental recovery curve, as is shown in Fig. 3 *B*. Let it be noted that the uniform disk model indeed accurately describes the experimental recovery curve. Because the recovery data results from integrating the fluorescence signal over the entire bleached disk, there is only a very small level of noise present in the experimental data.

RESULTS AND DISCUSSION

To fully examine and validate the new FRAP model, the influence of the different model parameters—the bleaching parameter K_0, the interline distance Δy, and the radius of the bleached disk w—on the measured diffusion coefficient D have to be examined.

The bleaching parameter K_0

If the uniform disk model is correct, the measured diffusion coefficient D should not be dependent on the bleaching depth, which is directly related to the bleaching parameter K_0 according to Eq. 9. Therefore, we have bleached in the FD167 solution with 30% (w/w) glucose, disks of constant radius $w = 12.5$ μm (which is a correct value as will be shown further on) but with different zoom settings to obtain a series of different K_0 values. The measured diffusion coefficient versus the corresponding K_0 value is shown in Fig. 4 *A*. The experiments have been evaluated both with and without taking the broadening of the bleaching disk with increasing bleaching depth into account, as predicted by Eq. 10. Without the correction for the radius w, there is a slight decrease of the measured diffusion coefficient D with increasing bleaching depth because of an underestimation

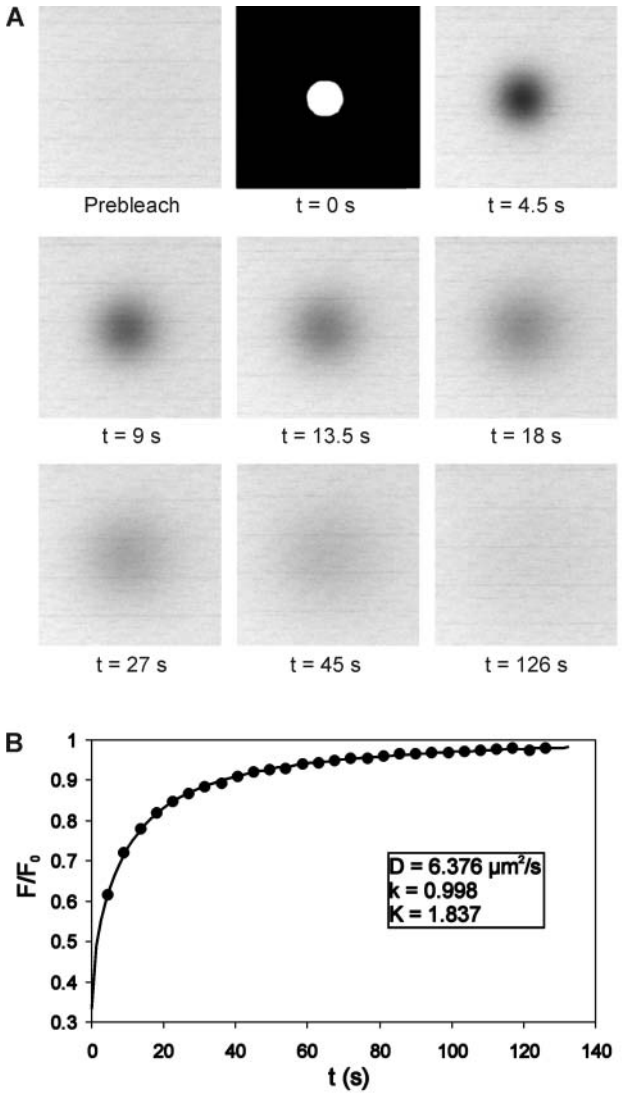

FIGURE 3 (*A*) A FRAP experiment is performed on the FD167 solution with 30% glucose (w/w). An image sequence is recorded of 30 images at regular time intervals of 4.5 s. The first image shows the sample before bleaching, the so-called *prebleach image*. When the second image is scanned, the bleaching software is activated and a user-defined disk is bleached. Next, the laser intensity is switched back to its previous level to record the recovery over multiple images at regular time intervals. (*B*) A dedicated image processing program extracts the recovery curve from the image sequence, as explained in the main text. The experimental data are indicated by black circles (●). A best fit of the model (*solid line*) finally yields the translational diffusion coefficient D, the mobile fraction k, and the bleaching parameter K_0.

of the radius w. Taking Eq. 10 into account for $r_0 = 3.5\ \mu$m nicely eliminates this dependency, whereas the correction for $r_0 = 1.4\ \mu$m is clearly insufficient. This result supports other observations from unrelated bleaching experiments that for fluorescein-labeled probes, the lateral resolution (and very likely the axial resolution as well) increases considerably at bleaching intensities compared to the resolution at imaging intensities. This increase in resolution is most likely due to the saturation of fluorescein at high bleaching intensities (Visscher et al., 1994; Song et al., 1995). A detailed study on the bleaching kinetics of fluorescein in combination with a high-intensity diffraction-limited bleaching beam would be necessary to examine this peculiar behavior, but is beyond the scope of this manuscript. It is also important to note from the uncorrected values in Fig. 4 *A* that, for $0.5 \leq K_0 \leq 2$, the variation of the diffusion coefficient is smaller than the experimental standard deviations (SDs). Therefore, we suggest that within the experimental accuracy, Eq. 10 can be neglected in practice for $0.5 \leq K_0 \leq 2$.

The experiments from this section can also be used to check if the bleaching kinetics can be described by a first-order reaction, as was assumed in the derivation of the model. As discussed in the Theory section, the bleaching parameter can be written in terms of the zoom setting Z:

$$K_0 = \frac{Z^2 \alpha I_{0b}}{v_0 \Delta y_0}.$$

If two disks of the same radius w are bleached in the same sample with identical bleaching intensity but with a different zoom setting Z_1 and Z_2, it follows that, if first-order kinetics are valid, the ratio of the two fitted K_0 values should be equal to

$$\frac{K_{01}}{K_{02}} = \left(\frac{Z_1}{Z_2}\right)^2. \tag{16}$$

The K_0 values from the experiments above can be used to verify Eq. 16 since the radius of the bleaching disk and bleaching intensity were held constant whereas the different bleaching depths were obtained by changing the zoom setting. The results are shown in Fig. 4 *B* where Eq. 16 was calculated for each measurement with regard to the measurement with lowest zoom setting and K_0 value. A linear fit to these data shows there is a good correspondence to Eq. 16.

Finally we would like to note that because of the presence of experimental noise, the accuracy of the measurements will decrease with decreasing bleaching depth (i.e., decreasing K_0 value). This is true for all FRAP experiments, regardless of the model. The more bleaching that has been induced, the larger the recovery interval will be and the less the presence of noise will affect the recovery curve. This can be verified by inspection of the error flags in Fig. 4 *A*.

The interline distance Δy

In the model it is assumed that the disk is uniformly bleached. As explained in Appendix B, for a Gaussian PSF this condition is theoretically met if $\Delta y \leq 0.5 r_0$. The distance between the adjacent lines Δy when scanning an image with the CSLM is directly determined by the electronic zoom setting. For the 10× NA 0.45 objective lens used in this study, $\Delta y = 2.115\ \mu$m at zoom 1, whereas at zoom setting Z, this becomes

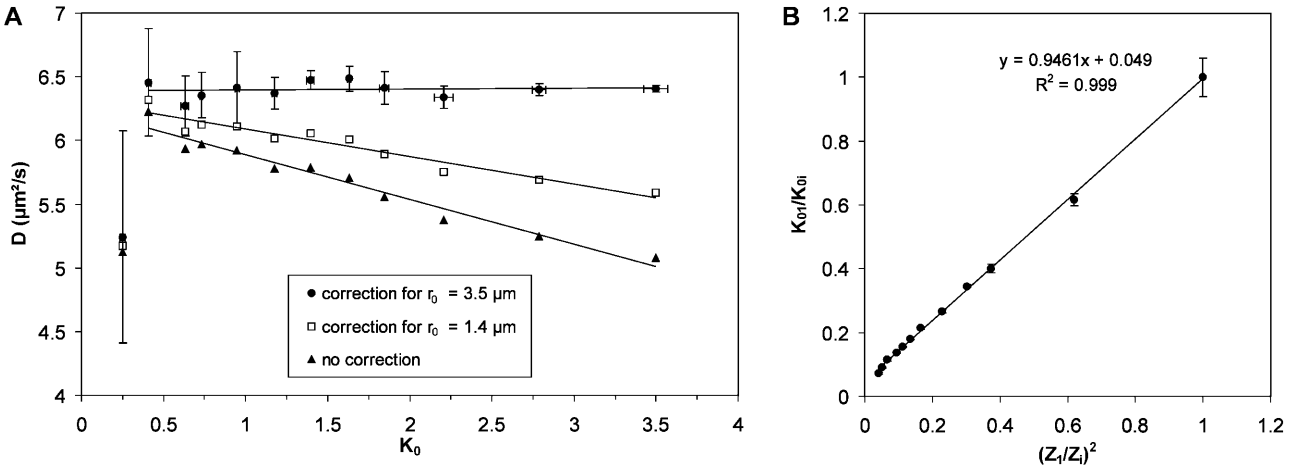

FIGURE 4 (*A*) FRAP measurements have been performed ($w = 12.5$ μm) on the solution of FD167 in 30% (w/w) glucose, for different bleaching depths (i.e., different K_0 values). All data are the result of 5–7 measurements and the error flags are the corresponding SD values. For clarity, the error flags are only shown for one of the data series, but are virtually the same for both other series. The black triangles (▲) are the results when Eq. 10 is not taken into account (no correction for the increasing radius with increasing bleaching depth). Because of an underestimation of the real bleaching radius, the measured diffusion coefficient decreases with increasing K_0 value. The white squares (□) are the results when Eq. 10 is taken into account for $r_0 = 1.4$ μm and the black circles (●) for $r_0 = 3.5$ μm. The solid lines are linear fits to the different data series. It is clear that the resolution at imaging intensities, $r_0 = 1.4$ μm (see Methods), is insufficient to correct for the dependency on K_0, confirming other observations that the effective radial resolution increases considerably at bleaching intensities for fluorescein-labeled probes. (*B*) As explained in the main text, the relationship $K_{01}/K_{0i}=(Z_1/Z_i)^2$ should be valid in the case of first-order bleaching kinetics. A linear fit to the experimental data shows this to be true in good approximation.

$$\Delta y = \frac{2.115}{Z}\,\mu\text{m}.$$

Hence, it is possible to verify experimentally to what extent the measurements are independent of the interline distance by performing FRAP experiments on the same solution with different zoom settings.

The results for D as a function of the zoom setting are shown in Fig. 5 *A*. The radius of the bleached disk was held constant at 15 μm (which is a correct value as will be shown in the next section). The horizontal line shows the mean value of all measurements. As can be seen, the measured diffusion coefficient is independent of the zoom setting for at least down to zoom 3, which corresponds to an interline distance of $\Delta y = 0.705$ μm. At lower zoom settings no sufficient bleaching could be obtained for meaningful measurements, even at maximum laser intensity. For the 10× objective lens, the radial resolution is 1.4 μm, although at bleaching intensities the effective resolution seems to be rather 3.5 μm as discussed in the previous section. Hence we have experimental proof that the measurements are independent of the interline distance for at least up to $0.2r_0$, which is in agreement with what is expected theoretically. Larger interline distances will, in practice, not occur very often because of insufficient bleaching at low zoom settings.

The radius *w* of the bleached disk

As discussed in the Theory section, the radius w of the bleached disk should be sufficiently large compared to the radial resolution r_0 of the bleaching PSF. Therefore, we have performed FRAP experiments on the same solution, FD167 with 40% (w/w) glucose, with increasing values for the radius w, ranging from 5.7 μm to 20.8 μm.

As can be seen from Fig. 5 *B*, the measured D values are independent of the radius in the region $w = 12.5$ μm to 21 μm. For smaller values of w it is clear that the discontinuous approximation is not valid any more. Therefore, we have always bleached disks with a radius between 12.5 μm and 15 μm, which corresponds to ~4× the bleaching resolution in fluorescein sampler. For much larger values of the radius w, deviations from the 2-D approximation are likely to occur because of an increasing contribution to the fluorescence recovery by diffusion in the z-direction.

Validation of the model

Having determined the ranges in which the model parameters K_0, Δy, and w may vary, it is now possible to test the ability of the new model to accurately measure diffusion coefficients. According to the Stokes-Einstein equation, a linear relation should be found between the translational diffusion coefficient D (m^2/s) and the reciprocal value of the dynamic viscosity η (Ns/m^2),

$$D = \frac{kT}{6\pi\eta r_H}, \tag{17}$$

where r_H is the hydrodynamic radius (m) of the diffusing molecules, k the Boltzmann constant (1.38×10^{-23} J/K), and T the absolute temperature (K). Fig. 6 *A* shows the

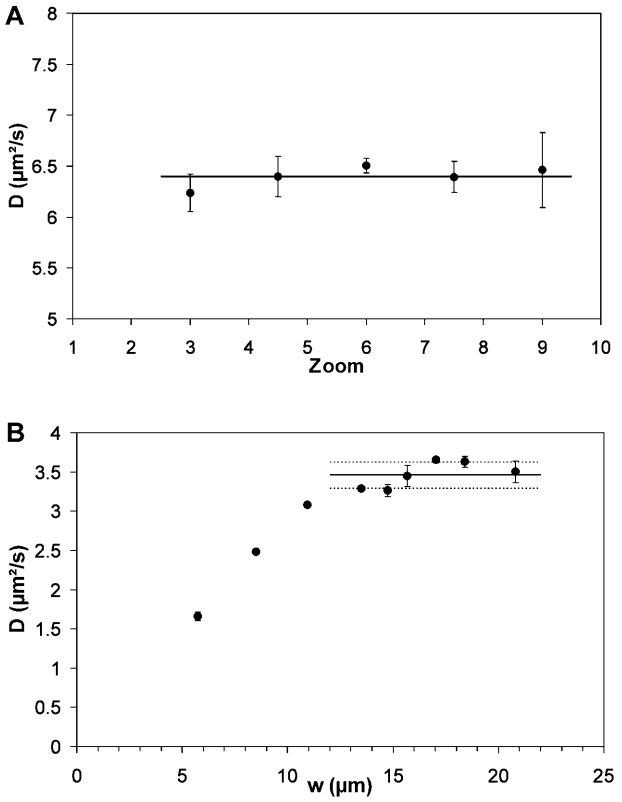

FIGURE 5 (*A*) The zoom setting on a CSLM determines the interline distance Δy for a given objective lens, which must be small enough for the uniform disk model to be valid. On our instrument, Δy is 2.115 μm at zoom 1 for the 10× objective lens and becomes $\Delta y/Z$ at zoom Z. Experiments have been performed on the FD167 solution with 30% (w/w) glucose, with a constant disk radius of 15 μm and different zoom settings: $Z = 3$, 4.5, 6, 7.5, and 9. The results are shown in the graph where each circle (●) is the mean result of 4–5 measurements and the error flags are the corresponding SD values. The horizontal line indicates the mean of all measurements. As can be seen, there is no dependency on the zoom setting within the experimental accuracy, for at least down to zoom 3. (*B*) For the uniform disk model to be valid, the radius w of the bleaching disk should be sufficiently large compared to the resolution r_0 of the bleaching PSF. FRAP measurements have been performed using different radii on the FD167 solution with 40% (w/w) glucose. The results for the diffusion coefficient D as a function of the radius w are shown in the graph. Each dot is the mean of five measurements and the error flags are the corresponding SD values. The diffusion coefficient D becomes independent of w starting from approximately $w = 12.5$ μm. The solid horizontal line indicates the mean value of the six measurements with $w \geq 12.5$ μm and the dashed lines indicate the corresponding SD value.

measured diffusion coefficient as a function of the reciprocal dynamic viscosity of the FITC-dextran glucose solutions. A good linear relationship is found between D and $1/\eta$, as predicted by Eq. 17.

Additionally, the ability of the uniform disk FRAP method to determine correctly absolute diffusion coefficients can be verified by comparing the measured values to their theoretical estimates. The hydrodynamic radius r_H of the FITC-dextrans can be estimated from a previously reported empirical relation (De Smedt et al., 1994; De Smedt, 1995),

$$r_H = 0.015 M_w^{0.53\pm0.02}, \quad (18)$$

where the molecular weight M_w is expressed in g/mol and r_H in nm. Based on Eq. 18, the FITC-dextrans used in this study have a hydrodynamic radius of 32.8 nm (FD2000), 15.1 nm (FD464), and 8.8 nm (FD167). Knowing r_H and η, a theoretical estimate of the diffusion coefficient of the FITC-dextrans can be made with Eq. 17. A parity plot is presented in Fig. 6 *B* showing the theoretically estimated values of the diffusion coefficients versus those actually measured. The solid line corresponds to Eq. 18 using the exponent of 0.53, whereas the dashed lines are calculated for exponent values of 0.51 and 0.55. As can be seen, there is a good correspondence between the measured values and their theoretical estimates. Considering Eq. 18 was determined from unrelated FRAP experiments on FITC-dextrans using a different FRAP model and a different instrument, these results prove the model is able to accurately determine the absolute values of the translational diffusion coefficients.

In addition we have measured the diffusion coefficient values of three watery solutions (FD2000, 37-nm, and 89-nm polystyrene nanospheres) by dynamic light scattering. The results for the diffusion coefficients are 6.16 ± 0.68 $\mu m^2/s$ for FD2000, 12.46 ± 0.70 $\mu m^2/s$ for the 37-nm spheres, and 5.19 ± 0.12 $\mu m^2/s$ for the 89-nm spheres. The diffusion coefficients of the same solutions were measured with the new FRAP technique as well: 6.43 ± 0.09 $\mu m^2/s$ for FD2000, 11.37 ± 0.58 $\mu m^2/s$ for the 37-nm spheres, and 5.68 ± 0.09 $\mu m^2/s$ for the 89-nm spheres. It is clear that the results from both techniques are in close agreement, giving additional proof that the new FRAP model is able to accurately measure absolute translational diffusion coefficients.

FRAP measurements with the CSLM in bovine vitreous and cystic fibrosis sputum

The eye is an ideal target for DNA therapy because it is easy to reach for treatment. DNA packed in viruses or nonviral nanoparticles can be administered by intravitreal injection. However, as the retinal epithelial cells are situated at the back of the eye, it has to be examined whether large molecules and nanoparticles can diffuse through the vitreous toward the target cells. A similar question arises when one wants to deliver drugs to the lungs, such as for treatment of CF, where the mucus may hinder the transport of therapeutics to the underlying lung cells.

As a first application, the new FRAP model, which is well-suited for measurements in bulk 3-D samples, was used to evaluate the effect of the size of macromolecules on their diffusion through both bovine vitreous and CF sputum. FITC-dextran solutions were injected into the vitreous gel and were observed to spread freely throughout the sample, resulting in a rather homogeneous fluorophore distribution.

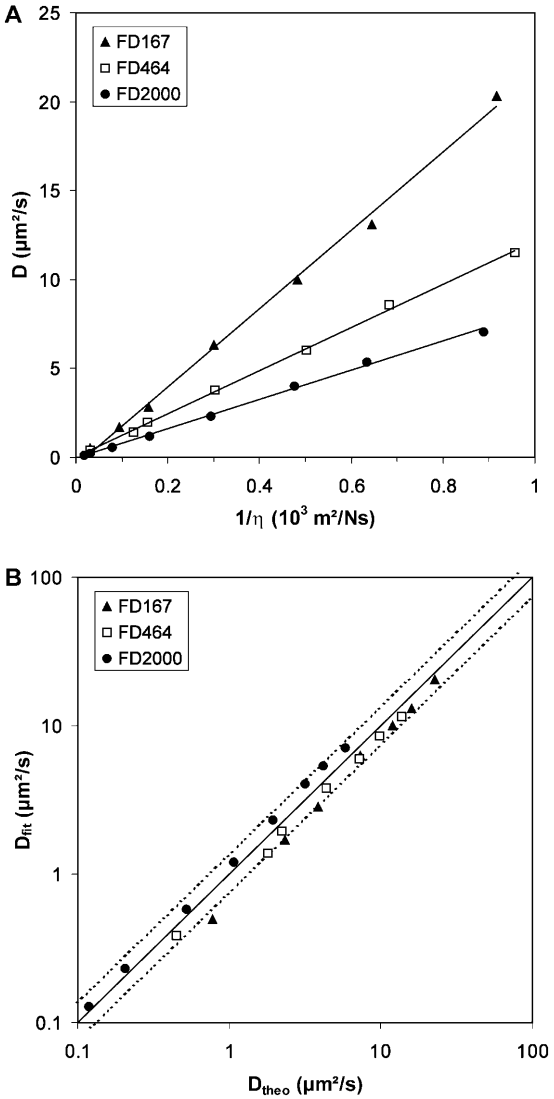

FIGURE 6 (*A*) The uniform disk model is verified with the Stokes-Einstein relation. FRAP measurements have been performed on FITC-dextrans solved in glucose solutions. A linear relationship between the measured diffusion coefficient D and the reciprocal viscosity is found, as predicted by the Stokes-Einstein equation. (*B*) Using Eqs. 17 and 18, the diffusion coefficient values of the FITC-dextran solutions can be estimated. The parity graph shows the measured diffusion coefficients D_{fit} versus the estimated values D_{theo}. The solid line has been calculated from Eq. 18 with an exponent of 0.53 and the dashed lines correspond to the exponent values of 0.51 and 0.55. As almost all measured diffusion coefficients fall within these limits, this proves the model can be used to accurately measure absolute translational diffusion coefficients.

When mixing the CF sputum with FITC-dextrans, however, a more heterogeneous distribution was obtained (see Fig. 7 *A*). For comparison, the CF sputum was also mixed with fluorescent nanospheres (see Fig. 7 *B*). While the FITC-dextrans seemed to be located between the biopolymers of the sputum, the polystyrene nanospheres did rather adsorb to the biopolymers, probably due to hydrophobic interactions. A similar observation has already been reported for polystyrene nanospheres mixed with cervical mucus (Olmsted et al., 2001). FRAP measurements did indeed reveal substantial immobile fractions of 38% for the 37-nm spheres and 56% for the 89-nm spheres (see Fig. 7, *C* and *D*).

The results of the FRAP measurements are shown in Table 1. A complete fluorescence recovery in vitreous for all FITC-dextrans ($k \approx 1$) was observed, suggesting that the molecules did not strongly chemically interact with the biopolymers. The diffusion coefficient values of FD167, FD464, and FD2000 in vitreous decreased, respectively, to 81 $\pm$ 3%, 74 $\pm$ 6%, and 65 $\pm$ 8%, compared to the value in buffer. In CF sputum, the diffusion coefficient values of FD167, FD464, and FD2000 decreased, respectively, to 34 $\pm$ 3%, 37 $\pm$ 3%, and 32 $\pm$ 2%. These results show that, in vitreous, increasing the size of the diffusing molecules induces a stronger sterical retardation by the meshwork. In CF sputum, on the other hand, the decrease in diffusion coefficient values of the FITC-dextrans seems to be rather independent of their size, indicating that the CF mucus does not impose a sterical hindrance on these molecules. These observations might be explained by the following hypothesis. The interfibrillar spaces of vitreous contain hyaluronic acid, which is a very efficient network-forming polymer (Scott, 1992; De Smedt et al., 1994; Lapcik et al., 1998) having a mesh size of tens of

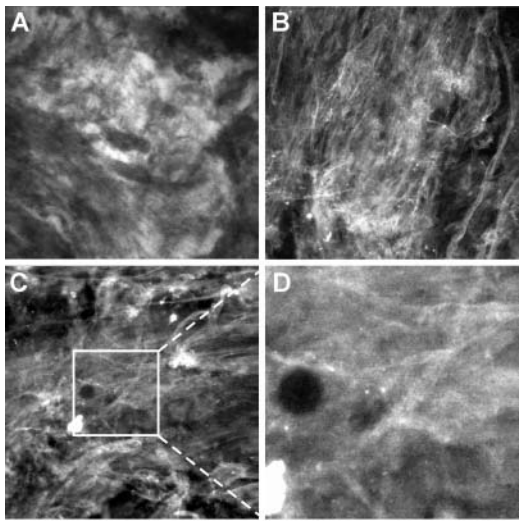

FIGURE 7 (*A*) Confocal image of cystic fibrosis sputum mixed with a FITC-dextran solution of 464 kDa molecular weight. The field of view (FOV) is 1047 μm $\times$ 1047 μm. (*B*) Confocal image of cystic fibrosis sputum mixed with 89-nm polystyrene nanospheres. The nanospheres tend to adsorb to the biopolymers of the CF sputum. The FOV is 1047 μm $\times$ 1047 μm. (*C*) Confocal image of cystic fibrosis sputum mixed with 89-nm spheres, recorded after the completion of a FRAP experiment in which a disk of radius 15 μm was bleached. Because of the presence of an immobile fraction, the recovery is incomplete and the bleached disk remains visible. The FOV is 524 μm $\times$ 524 μm. (*D*) Enlargement of the central part of image *C*. This image is the last image of the time-series recorded in the FRAP experiment. The FOV is 175 μm $\times$ 175 μm.

nanometers (De Smedt et al., 1994). The hyaluronic acid network sterically hinders the diffusion of the FITC-dextrans: the larger the molecule, the stronger the sterical hindrance. In contrast, the aqueous pores of the CF sputum network have a diameter of 100–400 nm (Sanders et al., 2000) and are filled with free (not entangled) biopolymers. This diluted biopolymer solution does not sterically hinder the diffusion of FITC-dextrans through the pores, but slows down the diffusion of the FITC-dextrans by a viscous drag, which is independent of the size of the diffusing FITC-dextrans.

CONCLUSIONS

We have presented a new 3-D FRAP model based on the bleaching of a uniform disk by the scanning beam of a confocal scanning laser microscope. Although the 3-D model has been derived for lenses of low numerical aperture, the corresponding 2-D expressions will be valid for high numerical aperture lenses as well if the sample thickness is small enough compared to the axial resolution of the bleaching beam. In addition, it has been shown that the model is equally valid for a stationary beam with a uniform radial intensity distribution.

Through a rigorous mathematical treatment of the bleaching process by a scanning beam, we have been able to show that the distance between two adjacent lines on the CSLM should be less than one-half the radial resolution of the scanning beam to obtain a uniformly bleached geometry. Additionally, the experiments have shown that the radius of the bleached disk should be $\sim 4\times$ the resolution of the bleaching PSF to avoid boundary effects. Therefore, the uniform disk approach in combination with low NA lenses is ideal for measurements on bulk samples such as biological or synthetic gels and solutions. In combination with high NA lenses, the corresponding 2-D expressions can be used for intracellular measurements as well if the cell thickness is small compared to the axial resolution of the bleaching beam.

The new FRAP model has the advantage of not requiring extensive mathematical or programming skills because the mathematical expressions are straightforward and can easily be programmed in a standard fitting routine. As the method of bleaching a disk by a scanning beam is readily available on commercial CSLMs, it offers a versatile tool for FRAP measurements and can be applied by anyone familiar with the CSLM instrument.

APPENDIX A: THE BLEACHING OF A LINE SEGMENT

Let us consider the case where the bleaching PSF, $I_b(x,y,z)$, is scanned across a single line with constant scanning speed v. As shown in Fig. 1 *A*, we take the x-axis to be parallel with the scanning direction. The scanned line is expressed by $y = Y$. While scanning across the line, the intensity of the illumination beam has zero intensity until it reaches position $x = a$, where the bleaching beam is switched on. At position $x = b$, the scanning beam is again switched off. Hence, the bleaching geometry is the line

$$B(x,y) = \begin{cases} L(x) \times \delta(y - Y) & a \le x \le b \\ 0 & x < a + x > b \end{cases},$$

where $\delta(y - Y)$ is the Dirac delta function, defined by the following properties: $\delta(y - Y) = 0$, if $y \neq Y$ and $\int_{-\infty}^{+\infty} f(y)\delta(y - Y)dx = f(Y)$. $L(x)$ is the function that describes the modulation of the light intensity over the line segment $[a,b]$ and has values between 0 and 1, where 0 means light switched off and 1 means maximum bleaching intensity. In fact, $B(x,y)$ expresses the behavior of the CSLM and $B(x,y) \times I_b(x,y,z)$ describes the real illumination modulation in the sample.

Because of the scanning process, the x-coordinate of the bleaching PSF is a function of time: $I_b(x - x(t),y - Y,z)$. If we take $t = 0$ at $x = a$, then explicitly $x(t) = vt + a$. If T is the time it takes for the scanning beam to cross the bleaching line with length $b - a$, the scanning speed is: $v = (b - a/T)$. T will be called the *bleaching time*. Now we want to know the bleaching effect at a location (x,y,z) when the bleaching of the line segment has completed. If we denote the initial concentration of fluorophores (i.e., before bleaching) as $C_0(x,y,z)$, the concentration after a bleaching time T, according to Eq. 1, is

$$C_b(x,y,z,T) = C_0(x,y,z)e^{-\alpha \int_0^T L(x(t))I_b(x-x(t),y-Y,z)dt}.$$

Expressing t in terms of $x(t)$ and renaming $x(t)$ as x' yields:

$$C_b(x,y,z,T) = C_0(x,y,z)e^{-(\alpha/v)\int_a^b L(x')I_b(x-x',y-Y,z)dx'}. \quad (19)$$

The integral in the exponent is nothing other than the 2-D convolution $K(x,y,z)$ of the bleaching geometry $B(x,y)$ with the bleaching PSF $I_b(x,y,z)$, as defined by Eq. 3. As can be seen, the scanning speed v determines the extent of bleaching for a *scanning* laser beam, rather than just the bleaching time T, as is the case for a *stationary* laser beam (Axelrod et al., 1976; Soumpasis, 1983; Blonk et al., 1993).

APPENDIX B: THE BLEACHING OF A 2-D GEOMETRY

In a CSLM, a 2-D geometry is bleached by scanning N subsequent line

TABLE 1 Measurement ($n = 5$) of the diffusion coefficient D ($\mu m^2/s$) and mobile fraction k by FRAP of FITC-dextrans in bulk 3-D samples: HEPES buffer, cystic fibrosis mucus, and bovine vitreous

	HEPES buffer		CF mucus		Bovine vitreous	
	$D \pm$ SD	$k \pm$ SD	$D \pm$ SD	$k \pm$ SD	$D \pm$ SD	$k \pm$ SD
FD167	18.80 ± 0.17	1.003 ± 0.002	6.43 ± 0.64	0.977 ± 0.014	15.23 ± 0.62	0.995 ± 0.018
FD464	10.97 ± 0.50	1.005 ± 0.003	4.09 ± 0.24	0.971 ± 0.016	8.07 ± 0.53	1.010 ± 0.026
FD20000	6.43 ± 0.09	1.000 ± 0.003	2.05 ± 0.11	0.900 ± 0.020	4.18 ± 0.53	0.984 ± 0.022

segments at a regular interline spacing Δy, as is shown in Fig. 1 *B*. Let $B(x,y)$ again describe the behavior of the CSLM to obtain the 2-D bleaching geometry. $B(x,y)$ is 0 outside the geometry's boundaries, and within it describes the laser intensity modulation as a function of the spatial coordinates:

$$B(x,y) = \begin{cases} L(x,Y)\delta(y-Y) & a_1 \le x \le b_1 \\ L(x,Y-\Delta y)\delta(y-(Y-\Delta y)) & a_2 \le x \le b_2 \\ \vdots & \\ L(x,Y-(N-1)\Delta y)\delta(y-(Y-(N-1)\Delta y)) & a_N \le x \le b_N \\ 0 & elsewhere \end{cases}$$

Again, we take the x-axis to be parallel with the scanning direction, whereas the origin is chosen arbitrarily. When scanning the first line at $y = Y$, a line segment is bleached from $x = a_1$ to $x = b_1$. Upon completion we know from Appendix A (Eq. 19) that the concentration of fluorophores is given by:

$$C_{b1}(x,y,z) = C_0(x,y,z)e^{-(\alpha/v)\int_{a_1}^{b_1} L(x',Y)I_b(x-x',y-Y,z)dx'}.$$

Next, the second line is scanned at a distance Δy below the first one and a line segment is bleached from $x = a_2$ to $x = b_2$. The concentration $C_1(x,y,z)$ is the initial situation for the second bleaching step. Upon completion of the second line, the concentration of fluorophores is given by

$$\begin{aligned} C_{b2}(x,y,z) &= C_{b1}(x,y,z)e^{-(\alpha/v)\int_{a_2}^{b_2} L(x',Y-\Delta y)I_b(x-x',y-Y+\Delta y,z)dx'} \\ &= C_0(x,y,z)e^{-(\alpha/v)[\int_{a_1}^{b_1} L(x',Y)I_b(x-x',y-Y,z)dx' + \int_{a_2}^{b_2} L(x',Y-\Delta y)I_b(x-x',y-Y+\Delta y,z)dx']}. \end{aligned}$$

If the bleaching geometry consists of N lines, the final concentration will be given by

$$C_{bN}(x,y,z) = C_0(x,y,z)e^{-(\alpha/v)\sum_{i=1}^{N}\int_{a_i}^{b_i} L(x',Y-(i-1)\Delta y)I_b(x-x',y-Y+(i-1)\Delta y,z)dx'}. \quad (20)$$

If the distance Δy is sufficiently small, the discrete summation can be approximated by an integral over a continuous variable y', leading to a double integral over the geometry G, expressed by $B(x,y)$:

$$C_b(x,y,z) = C_0(x,y,z)e^{-(\alpha/v)(1/\Delta y)\int\int_G L(x',y')I_b(x-x',y-y',z)dx'dy'}. \quad (21)$$

Again, the double integral is the convolution of $B(x,y)$ and the bleaching PSF $I_b(x,y,z)$, finally leading to Eq. 2. It is important to realize that Eq. 20 is always valid, whereas the continuous approximation Eq. 21 will only be valid if the interline distance Δy is sufficiently small compared to the resolution of the bleaching PSF. For a Gaussian PSF with resolution r_0, such as in Eq. 6, simulations of Eqs. 20 and 21 have shown that there is no noticeable difference between both expressions if $\Delta y \le 0.5r_0$. Under such conditions the geometry will be uniformly bleached because there is a sufficient overlap of the PSF for adjacent lines. On the other hand, for larger values of Δy, a wavelike pattern will result in the direction perpendicular to the line-scanning direction. In that situation, Eq. 21 is no longer valid, and Eq. 20 should be used instead. Finally, let it be noted, that the above reasoning can easily be extended to three (or more) dimensions.

APPENDIX C: FLUORESCENCE RECOVERY AFTER PHOTOBLEACHING OF A UNIFORM DISK AS OBSERVED BY THE CSLM

First consider an arbitrary axially symmetric initial concentration distribution $C_0(r,z)$. Fick's second law (Eq. 11) can be solved by first applying a Hankel transform to the radial coordinate r, followed by a Fourier transform to the axial coordinate z, finally leading to the general solution of

$$C(r,z,t) = \frac{1}{4\sqrt{\pi}(Dt)^{3/2}} \int_{z'=-\infty}^{+\infty}\int_{r'=0}^{+\infty} r'C_0(r',z')e^{-(z-z')^2/4Dt} \times e^{-(r^2+r'^2/4Dt)} I_0\left(\frac{rr'}{2Dt}\right)dr'\,dz', \quad (22)$$

where I_0 is the modified zero-order Bessel function. Solving Eq. 22 for the initial condition of Eq. 9 leads to the fluorophore concentration at a time t after bleaching of a uniform disk. This, however, is not what is observed directly by the CSLM, which ''looks'' at the sample with a detecting PSF $I_d(r,z)$. Again, if the radial resolution r_0 of the detecting PSF is much smaller than the bleaching disk's radius w, it can be shown that the total observed fluorescence within the disk $F_{tot}(t)$ can be calculated as if the detecting PSF is stationary at the disk's position and has a uniform light distribution of radius w,

$$F_{tot}(t) = 2\pi q \int_{z=-\Delta z_0}^{+\Delta z_0}\int_{r=0}^{+\infty} rI_d(r,z)C(r,z,t)dr\,dz, \quad (23)$$

where q is a constant factor taking all relevant attenuation and light collection factors into account. In a similar way as in previous work (Blonk et al., 1993), the finite size of the confocal pinhole for the fluorescence detection is taken into account in Eq. 23 by eliminating all light from planes above $z = \Delta z_0$ and below $z = \Delta z_0$. Substituting the result from Eq. 22 for the initial condition Eq. 9 into Eq. 23 and following a similar strategy as was used by Soumpasis (1983) finally leads to Eq. 12.

We thank Stephanie Quintelier and Philippe Keppens for their help with the FRAP experiments. We also thank Marc Leblans for mathematical support and Johan Van de Voorde and Koen Boussery for supplying the vitreous samples.

The financial support of the IWT-Vlaanderen and Tibotec is acknowledged with gratitude. Ghent University (BOF) is acknowledged for its support through instrumentation credits.

REFERENCES

Axelrod, D., D. E. Koppel, J. Schlessinger, J. Elson, and W. W. Webb. 1976. Mobility measurement by analysis of fluorescence photobleaching recovery kinetics. *Biophys. J.* 16:1055–1069.

Berk, D. A., F. Yuan, M. Leunig, and R. K. Jain. 1993. Fluorescence photobleaching with spatial Fourier analysis: measurement of diffusion in light-scattering media. *Biophys. J.* 65:2428–2436.

Blonk, J. C. G., A. Don, H. Van Aalst, and J. J. Birmingham. 1993. Fluorescence photobleaching recovery in the confocal scanning light microscope. *J. Microsc.* 169:363–374.

Braeckmans, K., S. C. De Smedt, C. Roelant, M. Leblans, R. Pauwels, and J. Demeester. 2003. Encoding microcarriers by spatial selective photobleaching. *Nature Mat.* 2:169–173.

Brown, E., A. Pluen, C. Compton, Y. Boucher, and R. K. Jain. 2000. Measurement of diffusion coefficients in spontaneous human tumors. *FASEB J.* 14:A167.

Campbell, R. B., D. Fukumura, E. B. Brown, L. M. Mazzola, Y. Izumi, R. K. Jain, V. P. Torchilin, and L. L. Munn. 2002. Cationic charge determines the distribution of liposomes between the vascular and extravascular compartments of tumors. *Cancer Res.* 62:6831–6836.

Chary, S. R., and R. K. Jain. 1989. Direct measurement of interstitial convection and diffusion of albumin in normal and neoplastic tissues by fluorescence photobleaching. *Proc. Natl. Acad. Sci. USA.* 86: 5385–5389.

Cho, M. J., and R. Juliano. 1996. Macromolecular versus small-molecule therapeutics: drug discovery, development and clinical considerations. *Trends Biotechnol.* 14:153–158.

Cogswell, C. J., and K. G. Larkin. 1995. The Specimen Illumination Path and its Effects on Image Quality. *In* Handbook of Biological Confocal microscopy, 2nd ed. J. P. Pawley, editor. Plenum Press, New York. pp.127–137.

Crank, J. 1975. The Mathematics of Diffusion, 2nd Ed. Clarendon Press, Oxford, UK.

Crystal, R. G. 1995. The gene as the drug. *Nat. Med.* 1:15–17.

De Smedt, S. C., A. Lauwers, and J. Demeester. 1994. Structural information on hyaluronic acid solutions as studied by probe diffusion experiments. *Macromolecules.* 27:141–146.

De Smedt, S. C. 1995. De invloed van het netwerk in hyaluronzuuroplossingen en dextraan-glycosidymethacrylaat-hydrogelen op de diffusie van macromoleculen. Ghent University. PhD thesis.

Edidin, M. 1992. Translational diffusion of membrane proteins. *In* The Structure of Biological Membranes. P. Yeagle, editor. CRC Press, Boca Raton, FL. pp.539–572.

Gordon, G. W., B. Chazotte, X. F. Wang, and B. Herman. 1995. Analysis of simulated and experimental fluorescence recovery after photobleaching. Data for two diffusing components. *Biophys. J.* 68:766–778.

Ishihara, A., and K. Jacobson. 1993. A closer look at how membrane proteins move. *Biophys. J.* 65:1754–1755.

Keller, H. E. 1995. Objective lenses for confocal microscopy. *In* Handbook of Biological Confocal Microscopy, 2nd Ed. J. P. Pawley, editor. Plenum Press, New York. pp.111–126.

Kubitscheck, U., P. Wedekind, and R. Peters. 1994. Lateral diffusion measurements at high spatial resolution by scanning microphotolysis in a confocal microscope. *Biophys. J.* 67:948–956.

Kubitscheck, U., P. Wedekind, and R. Peters. 1998. Three-dimensional diffusion measurements by scanning microphotolysis. *J. Microsc.* 192: 126–138.

Lapcik Jr., L., L. Lapcik, S. De Smedt, J. Demeester, and P. Chabrecek. 1998. Hyaluronan: preparation, structure, properties, and applications. *Chem. Rev.* 98:2663–2684.

Lopez, A., L. Dupou, A. Altibelli, J. Trotard, and J. Tocanne. 1988. Fluorescence recovery after photobleaching (FRAP) experiments under conditions of uniform disk illumination. *Biophys. J.* 53:963–970.

Meyvis, T. K. L., S. C. De Smedt, P. Van Oostveldt, and J. Demeester. 1999. Fluorescent recovery after photobleaching: a versatile tool for mobility and interaction measurements in pharmaceutical research. *Pharm. Res.* 16:1153–1162.

Olmsted, S. S., J. L. Padgett, A. I. Yudin, K. J. Whaley, T. R. Moench, and R. A. Cone. 2001. Diffusion of macromolecules and virus-like particles in human cervical mucus. *Biophys. J.* 81:1930–1937.

Peters, R., and U. Kubitscheck. 1999. Scanning microphotolysis: three-dimensional diffusion measurement and optical single-transporter recording. *Methods.* 18:508–517.

Pluen, A., Y. Boucher, S. Ramanujan, T. D. McKee, T. Gohongi, E. di Tomaso, E. B. Brown, Y. Izumi, R. B. Campbell, D. A. Berk, and R. D. Jain. 2001. Role of tumor-host interactions in interstitial diffusion of macromolecules: cranial vs. subcutaneous tumors. *Proc. Natl. Acad. Sci. USA.* 98:4628–4633.

Ramanujan, S., A. Pluen, T. D. McKee, E. B. Brown, Y. Boucher, and R. D. Jain. 2002. Diffusion and convection in collagen gels: implications for transport in the tumor interstitium. *Biophys. J.* 83:1650–1660.

Rojanasakul, Y. Y. 1996. Antisense oligonucleotide therapeutics: drug delivery and targeting. *Adv. Drug Del. Rev.* 18:115–131.

Saltzman, W. M., M. L. Radomsky, K. J. Whaley, and R. A. Cone. 1994. Antibody diffusion in human cervical mucus. *Biophys. J.* 66:508–515.

Sanders, N. N., S. C. De Smedt, and J. Demeester. 2000. The physical properties of biogels and their permeability for macromolecular drugs and colloidal drug carriers. *J. Pharm. Sci.* 89:835–849.

Sanders, N. N., E. Van Rompaey, S. De Smedt, and J. Demeester. 2001. Structural alterations of gene complexes by cystic fibrosis sputum. *Am. J. Crit. Care.* 164:486–493.

Sanders, N. N., E. Van Rompaey, S. C. De Smedt, and J. Demeester. 2002a. On the transport of lipoplexes through cystic fibrosis sputum. *Pharm. Res.* 19:451–456.

Sanders, N. N., S. C. De Smedt, S. H. Cheng, and J. Demeester. 2002b. Pegylated GL67 lipoplexes retain their gene transfection activity after exposure to components of CF mucus. *Gene Ther.* 9:363–371.

Scott, J. E. 1992. The chemical morphology of the vitreous. *Eye.* 6: 553–555.

Seksek, O., J. Biwersi, and A. S. Verkman. 1997. Translational diffusion of macromolecule-sized solutes in cytoplasm and nucleus. *J. Cell Biol.* 138:131–142.

Song, L., E. J. Hennink, I. T. Young, and H. J. Tanke. 1995. Photobleaching kinetics of fluorescein in quantitative fluorescence microscopy. *Biophys. J.* 68:2588–2600.

Soumpasis, D. M. 1983. Theoretical analysis of fluorescence photobleaching recovery experiments. *Biophys. J.* 41:95–97.

Torchilin, V. P. 2000. Drug targetting. *Eur. J. Pharm. Sci.* 11:S81–S91.

Tsay, T., and K. A. Jacobson. 1991. Spatial Fourier analysis of video photobleaching measurements, principles and optimization. *Biophys. J.* 60:360–368.

Umenishi, F., J. Verbavatz, and A. S. Verkman. 2000. cAMP-regulated membrane diffusion of green fluorescent protein-aquaporin 2 chimera. *Biophys. J.* 78:1024–1035.

Visscher, K., G. J. Brakenhoff, and T. D. Visser. 1994. Fluorescence saturation in confocal microscopy. *J. Microsc.* 175:162–165.

Wedekind, P., U. Kubitscheck, and R. Peters. 1994. Scanning microphotolysis: a new photobleaching technique based on fast intensity modulation of a scanned laser beam and confocal imaging. *J. Microsc.* 176:23–33.

Wedekind, P., U. Kubitscheck, O. Heinrich, and R. Peters. 1996. Line-scanning microphotolysis for diffraction-limited measurements of lateral diffusion. *Biophys. J.* 71:1621–1632.

Weers, J. G. 1998. Colloidal particles in drug delivery. *Curr. Opin. Coll. Inter.* 3:540–544.